Journal of ELECTRONIC MATERIALS, Vol. 40, No. 11, 2011
DOI: 10.1007/s11664-011-1749-z

Studies on Conducting Polypyrrole/Graphene Oxide Composites as Supercapacitor Electrode

SURAJIT KONWER,[1] RATAN BORUAH,[2] and SWAPAN K. DOLUI[1,3]

1.—Department of Chemical Sciences, Tezpur University, Napaam 784028, Assam, India. 2.—Department of Physics, Tezpur University, Napaam 784028, Assam, India. 3.—e-mail: dolui@tezu.ernet.in

An electrode material based on polypyrrole (PPy) doped with graphene oxide (GO) sheets was synthesized via *in situ* polymerization of pyrrole in the presence of GO in various proportions (5% and 10%). The synthesized samples were characterized by Fourier-transform infrared (FTIR) spectroscopy, ultraviolet–visible (UV–vis) absorption spectroscopy, scanning electron microscopy (SEM), transmission electron microscopy (TEM), thermogravimetric analysis (TGA), x-ray diffraction (XRD) analysis, and electrical conductivity measurements. FTIR spectroscopy and XRD revealed the interaction between GO and PPy. The direct-current (DC) electrical conductivity (75.8 S/cm) of the prepared composites was dramatically enhanced compared with pure PPy (1.18 S/cm). High specific capacitance of PPy/GO composite of 421.4 F/g was obtained in the potential range from 0 V to 0.50 V at 2 mA compared with 237.2 F/g for pure PPy by galvanostatic charge–discharge analysis. Incorporation of GO into the PPy matrix has a pronounced effect on the electrical conductivity and electrochemical capacitance performance of PPy/GO nanocomposites.

Key words: Polypyrrole, graphene oxide, electrical conductivity, capacitance, supercapacitor

INTRODUCTION

Recently, electrochemical capacitors, also known as supercapacitors, have attracted a great deal of interest as the best candidates to provide the high power and long durability needed for new energy devices such as hybrid peak-power sources in electric vehicles, back-up sources for various electrical devices, and uninterrupted power supplies for memory protection in computer electronics and cellular communication devices.[1–4] The main materials studied for supercapacitor electrodes are carbons, metal oxides, and conducting polymers.[5] Great attention has been focused on conducting polymer-based electrochemical capacitors owing to their remarkable merits such as high capacitive energy density and low material cost, based on materials such as polyaniline, PPy, poly(ethylenedioxythiophene), and polythiophene and its substituted counterparts.[6] Especially PPy has been considered as the most promising material for this application due to its excellent capacity for energy storage, easy synthesis, stability in air, higher conductivity, and lower cost than many other conducting polymers.[7–9] The main drawback of application of conducting polymers as supercapacitor electrodes is their poor stability during cycling because of swelling and shrinkage that may occur during doping/dedoping processes. This leads to mechanical degradation of the electrodes and weakening of their electrochemical performance.[10,11]

Combination of conducting polymer with various carbon materials has been attempted to reinforce the stability of the polymer composite as well as to improve the capacitance and conductivity of carbon-based supercapacitors. Gupta and Miura reported electrochemical polymerization of polyaniline/single-walled carbon nanotube composites, with the highest specific capacitance of 463 F/g obtained for 73 wt.% polyaniline.[12,13] Jang et al. synthesized

(Received May 4, 2011; accepted August 23, 2011; published online September 22, 2011)

polyaniline-coated carbon nanofibers by the one-step vapor deposition polymerization technique, and the maximum specific capacitance was 264 F/g when the thickness of the polyaniline layer was ca. 20 nm.[14] Rudge et al. reported fabrication of a conducting polymer/graphite fiber composite with PPy by using electrochemical polymerization of pyrrole on the surface of graphite fibers, with higher capacitance and conductivity.[15,16] Compared with other carbon fillers, GO is predicted to be an excellent support material due to its high surface area and remarkable mechanical stiffness.

Conducting polymer-based supercapacitors can be classified into three types.[1] Type I is a symmetric system where the same *p*-dopable conducting polymer is used at both electrodes of the capacitor. Type II is an asymmetric system based on two different *p*-dopable conducting polymers as electrode materials. Type III is a symmetric system based on a conducting polymer that can be used as both a *p*- and *n*-doped electrode material.

In this work we attempt to build a type I supercapacitor using two identical electrodes with the same conducting polymer composite material. We synthesised two composite PPy/GO electrodes by incorporation of GO into PPy through *in situ* polymerization of pyrrole. Structural morphology was investigated and characterization carried out by XRD, SEM, and TEM analysis. The effect of GO on the electrical and electrochemical capacitance performance of the PPy/GO composite for supercapacitor applications has been studied thoroughly. To the best of our knowledge, synthesis of PPy/GO functional composite electrodes and study of their electrical and electrochemical capacitance behavior have not been reported so far.

EXPERIMENTAL PROCEDURES

Pyrrole was obtained from Aldrich Co. and used without further purification. Natural graphite flake of size −50 + 100 BS mesh, hydrochloric acid (HCl), sulfuric acid (H_2SO_4), nitric acid (HNO_3), and anhydrous ferric chloride ($FeCl_3$) were obtained from Merck and used as received. The solvent methanol (CH_3OH) was distilled before use. Acetonitrile (CH_3CN) was obtained from Merck and purified by standard methods. Lithium perchlorate ($LiClO_4$) was obtained from Fluka and used as received. For all purposes double-distilled water was used.

FTIR spectra were recorded by a Impact 410 (Nicolet, USA) using KBr pellets. The UV–vis absorption spectroscopy of the samples in N-methyl-2-pyrrolidone was recorded using a Shimadzu UV-2550 UV–vis spectrophotometer in the range of 300 nm to 800 nm. The surface morphology of the composites was observed by SEM (JSM-6390LV, JEOL, Japan). The surface of the sample was coated with platinum before SEM analysis. TEM measurements were conducted on a Philips CM 200 microscope at 200 kV. TEM samples were prepared by dispensing a small amount of dry powder in ethanol. Then, one drop of the suspension was dropped on 300 mesh copper TEM grids covered with thin amorphous carbon films. TGA was performed using a TG 50 thermogravimetric analyzer (Shimadzu, Japan) in the temperature range of 25°C to 973°C with a heating rate of 10°C/min under a nitrogen flow rate of 30 mL/min to study the thermal degradation of the samples. XRD study was carried out at room temperature (ca. 25°C) on a Rigaku x-ray diffractometer with Cu K_α radiation (λ = 0.15418 nm) at 30 kV and 15 mA using a scanning rate of 0.050°/s in the 2θ range of 10° to 70°.

Preparation of Graphene Oxide

GO was synthesized from natural graphite by a modified Hummers method. In a 500-mL beaker, 5 g graphite and 2.5 g $NaNO_3$ were mixed with 120 mL concentrated H_2SO_4. The mixture was stirred for 30 min in the temperature range of 0°C to 5°C. During stirring, 15 g $KMnO_4$ was slowly added to the suspension and the temperature was maintained to below 20°C. After addition of $KMnO_4$, the reaction mixture was then stirred at 30°C until it became pasty and the color became light brownish. Finally, 150 mL H_2O was slowly added to the paste with vigorous stirring. The diluted yellow suspension was again stirred at 98°C for 24 h. Finally 50 mL 30% H_2O_2 was added. The whole reaction mixture was washed by centrifuging with 1.5 M HCl followed by distilled water for 8 to 10 times and filtered to obtain gray GO sheets.

Preparation of Polypyrrole/Graphene Oxide Composite

The polypyrrole/graphene oxide (PPy/GO) composites were prepared by *in situ* polymerization involving pyrrole and graphite oxide. In a three-necked round-bottomed flask, GO was dispersed in 50 mL methanol by ultrasonication for 30 min. Then, pyrrole (0.2 M) was dissolved in the dispersed solution and ultrasonication was continued for another 30 min. The weight ratio of pyrrole to GO was varied as 100:5 and 100:10, and the resulting composites were designated as PPy/GO (5%) and PPy/GO (10%). Then 2.5 M $FeCl_3$ solution (in 20 mL methanol) was added dropwise to the mixture of pyrrole and GO in a temperature range close to 0°C to 5°C under vigorous stirring for 6 h. The polymer composite so obtained was filtered, washed with water and methanol until the solution became colorless, and dried in vacuum.

Electrochemical Measurements

Using a compression-molding machine, pellets of composite electrodes were made. High pressure was applied (1.5 ton to 2 ton) to the sample to obtain a hard round pellet (1.5 cm diameter, 2 mm breadth).

Two-electrode capacitor cells were constructed with electrolyte poly(ethylene oxide) as separator using a sandwich-type construction (electrode/separator/electrode) with a silver paste current collector. The electrodes were prewetted with electrolyte before use. The capacitor performance was characterized by means of galvanostatic charge–discharge tests using an Autolab PGSTAT302N at room temperature. In case of the three-electrode cell, the working electrode was the PPy/GO composite, platinum wire was the counterelectrode, and standard calomel electrode (SCE) was used as the reference electrode.

RESULTS AND DISCUSSION

The PPy/GO composite was prepared by *in situ* oxidative polymerization. The monomer pyrrole may get adsorbed on the surface and gallery of GO. The pyrrole adsorbed on the GO, as well as remaining as free aniline, polymerizes in the presence of the oxidizing agent $FeCl_3$ to yield PPy/GO composite. The functional groups –OH, –COOH, and epoxy exist on the surface and pores of the GO, promoting H-bonding of the GO to the PPy backbone (Fig. 1).

FTIR spectra of GO, PPy, and PPy/GO are shown in Fig. 2. For the PPy sample, the absorption peaks at 1443 cm^{-1}, 1581 cm^{-1}, and 3433 cm^{-1} are associated with the C-C, C-N, and N-H stretching vibration in the polypyrrole ring. The absorption peaks located at 2926 cm^{-1} and 2855 cm^{-1} are ascribed to asymmetric stretching and symmetric vibrations of CH_2, respectively.[17] In the FTIR spectrum of GO the broad peak at 3434 cm^{-1} and a peak at 1730 cm^{-1} correspond to O-H stretching vibration and strong carbonyl (C=O) stretching, respectively. The peaks at 1222 cm^{-1} and 1406 cm^{-1} correspond to C-O-C and C-OH stretching vibration, respectively.[18] The peak at 1077 cm^{-1} corresponds to C-O stretching vibration, indicating the presence of epoxide group in the GO layers. In the spectrum of the PPy/GO composites, the characteristic absorption peak of C=O group has been downshifted to 1728 cm^{-1}, which is probably due to π–π interaction between the GO layers and aromatic polypyrrole rings. The characteristic peaks of PPy at 1587 cm^{-1} and 1450 cm^{-1} suggest the presence of PPy in the PPy/GO composite.

The UV–visible spectrum of PPy shows weaker absorption at around 215 nm and stronger absorption at around 505 nm. The first absorption band is associated with the π–π^* transition while the second is assigned to the polaron state of PPy (Fig. 3b). The sharp UV–vis spectrum of GO was observed at

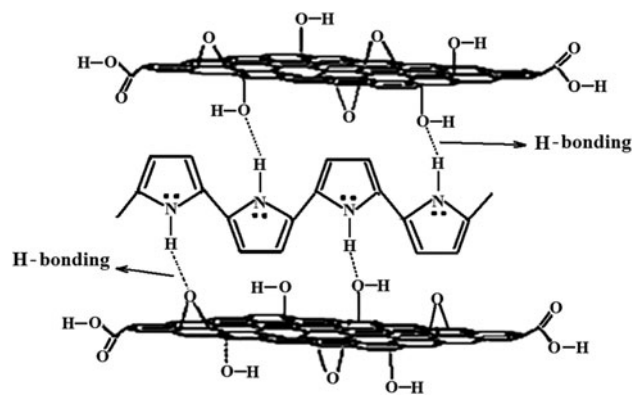

Fig. 1. Schematic representation depicting interaction of GO sheet and PPy chain.

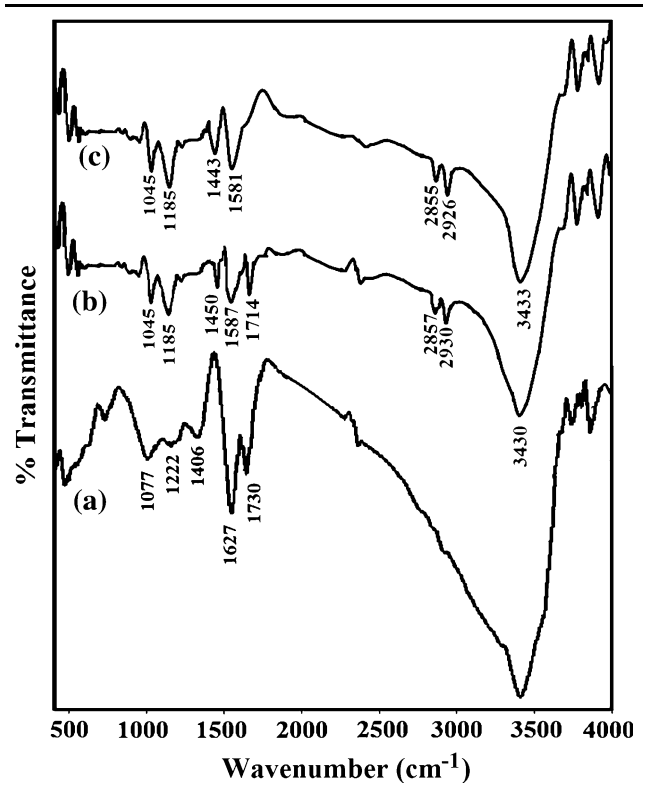

Fig. 2. FTIR spectra of (a) GO, (b) PPy/GO, and (c) PPy.

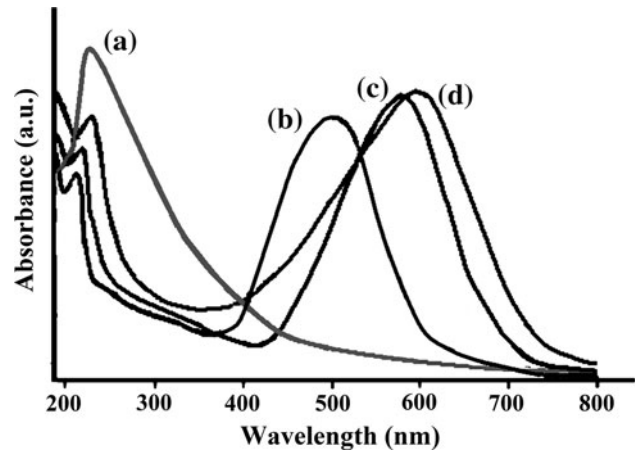

Fig. 3. UV–visible spectra of (a) GO, (b) PPy, (c) PPy/GO (5%), and (d) PPy/GO (10%).

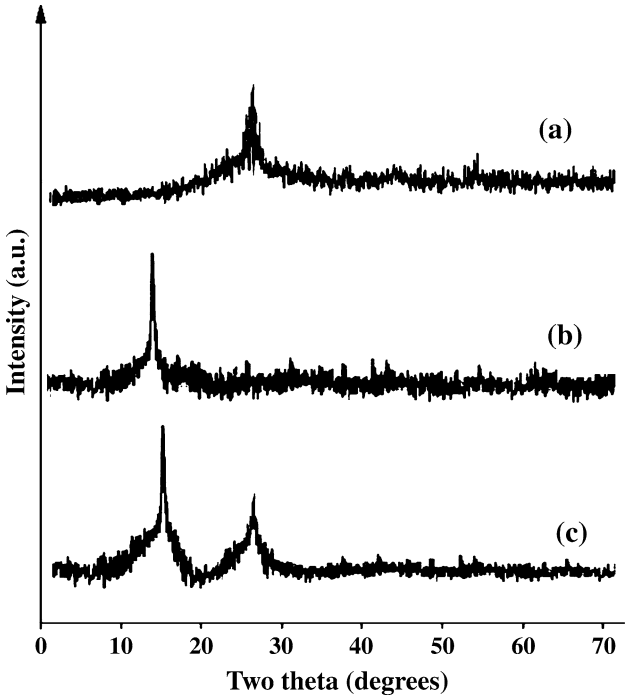

Fig. 4. XRD analysis of (a) PPy, (b) GO, and (c) PPy/GO composite.

235 nm (Fig. 3a). The PPy/GO composite shows a similar spectrum to pure PPy, where the signal at 505 nm is shifted to 580 nm and 595 nm for PPy/GO (5%) and PPy/GO (10%), respectively. This indicates that the PPy is also in a polaronic state in the synthesized PPy/GO composite. Moreover, the peaks at 218 nm and 220 nm are related to conjugation of the molecule. GO assists the polymerization in such a way that it maintains a higher conjugation length in the chain of the PPy itself, and there may have been some coupling between the conjugation length of the PPy and GO. In addition, functional groups such as –OH and –COOH exist on the surface and pores of the GO after acid treatment and could promote adsorption of molecular chains and monomers onto the pores. Moreover, the π–π stacking between the polymer backbone and the GO sheets may also contribute to extend the conjugation length of the polymer composite. The characteristic redshift of PPy/GO nanocomposites due to the extended conjugation length of PPy chains and high degree of incorporation of GO is clearly shown in Fig. 3. The enhanced DC electrical conductivity of the PPy/GO composite also further supports the redshift behavior of the composite.

Figure 4 shows the XRD pattern of pure PPy, GO and PPy/GO composite. The XRD pattern of pure PPy, which had a peak at about $2\theta = 26°$, shows semicrystalline nature. In GO, a peak at $2\theta = 13°$ is observed, which is similar to that reported in earlier literature.[19] This indicates the formation of layer-like GO sheets. The PPy/GO composite exhibits two peaks at $2\theta = 13°$ for GO and $2\theta = 26°$ for PPy, indicating incorporation of GO into the PPy matrix.

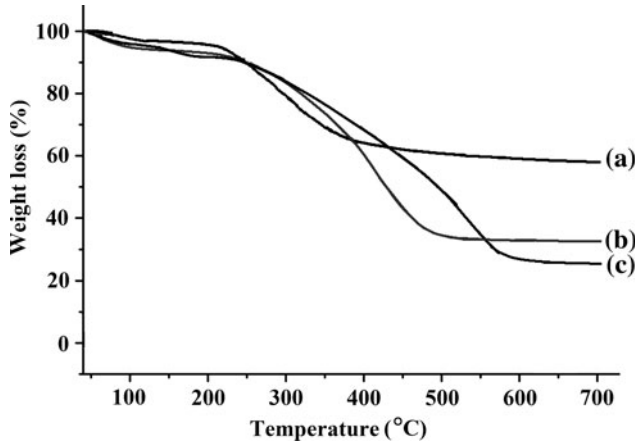

Fig. 5. TGA of (a) GO, (b) PPy/GO, and (c) pure PPy.

Thermogravimetric profiles of PPy, GO, and PPy/GO composites are given in Fig. 5. The initial weight loss for all samples in the temperature range of 90°C to 115°C reflects loss of moisture from the samples. The major weight loss of GO at the temperature range of 215°C to 310°C reveals the presence of functional groups on the surface of the GO sheets. During this dramatic weight loss of GO (Fig. 5a), most of the oxygen-containing functional groups are removed from the GO, and the material becomes single graphene and expanded graphite sheets.[20] The residual weight of the GO is about 68 wt.%, indicating that at least 32 wt.% functional groups existed on GO before thermal treatment by TGA.

In PPy/GO composite (Fig. 5b), the weight loss near 210°C is probably due to removal of the oxygen-containing functional groups. After 250°C, major weight loss occurred due to decomposition of the PPy from the composite. Finally at 450°C, almost 24% weight loss for GO-based PPy composite was observed.

SEM images of pure PPy, GO, and PPy/GO are shown in Fig. 6. The GO inherits the layer-by-layer and network structure with denser stacking, while the SEM image of PPy shows the hemispherical nature of the polymer. In the SEM micrographs of PPy/GO composite, smooth surfaces are observed. Since the polymers grow in the pores and galleries of GO, it is difficult to distinguish the individual phases, i.e., GO and PPy, in the PPy/GO composite from the SEM micrograph.

The morphology of GO is shown in the TEM image of Fig. 7a. The GO prepared here has a typically curved, layer-like structure with ~5 nm to 10 nm thickness. For PPy/GO composite (Fig. 7b) the TEM image shows that all the GO sheets are homogeneously coated with polymer and that the PPy mainly grows on the surface or intercalates between the GO sheets. SEM and TEM images reveal that the chemically modified GO and the PPy formed a uniform composite with the PPy absorbed on the GO surface and/or filled between the GO nanosheets.

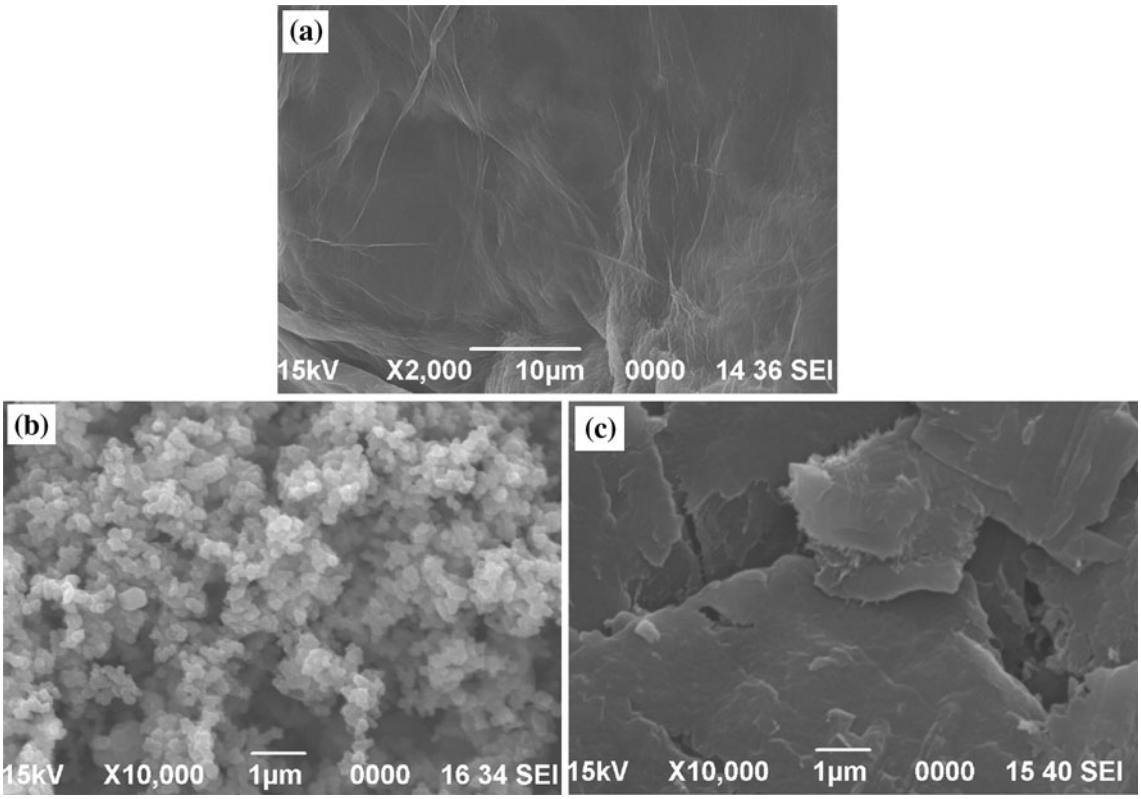

Fig. 6. SEM images of the (a) GO, (b) PPy, and (c) PPy/GO composite.

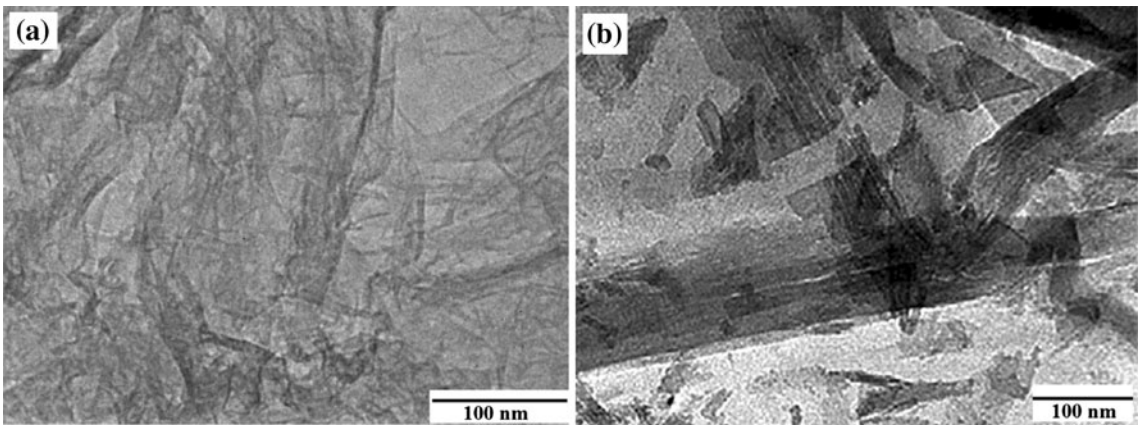

Fig. 7. TEM image of (a) GO and (b) PPy/GO composite.

The DC electrical conductivity of the conducting composite was measured by using a four-probe resistivity measurement system. The conductivity of the PPy/GO composite was calculated using the following equations:

$$\rho = \rho_0 / G_7(W/S), \tag{1}$$

$$G_7(W/S) = (2S/W)\ln 2, \tag{2}$$

$$\rho_o = (V/I)2\pi S, \tag{3}$$

$$\sigma = 1/\rho_0, \tag{4}$$

where G_7 (W/S) is a correction divisor which is a function of sample thickness and probe spacing; I, V, W, and S are the current (A), voltage (V), thickness of the pellet (cm), and probe spacing (cm), respectively.

Table I. Conductivity of the PPy and PPy/GO composites at various temperatures

Temperature (°C)	Conductivity (S/cm)			
	GO	PPy	PPy/GO (5%)	PPy/GO (10%)
25	0.5	0.30	41.2	62
30	–	0.17	37.8	58.2
50	–	0.25	39.3	60.5
70	–	0.38	44	64.2
90	–	0.57	48.7	69.4
110	–	1.13	57.2	74
130	–	1.18	58.6	75.2
150	–	1.18	59	75.8

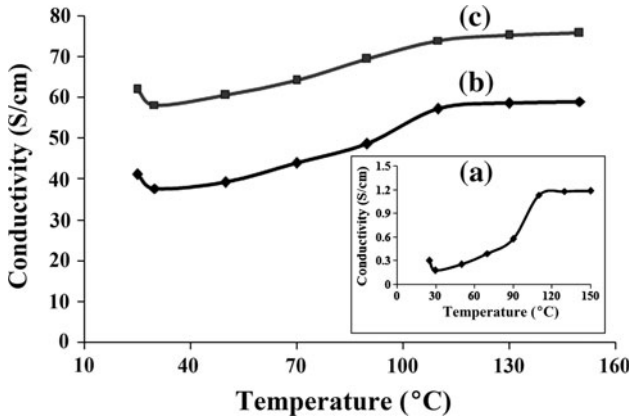

Fig. 8. Conductivity versus temperature curve of (a) PPy, (b) PPy/GO (5%), and (c) PPy/GO (10%) composites.

The electrical conductivity of the PPy, GO, and the composite material were determined and are listed in Table I. The GO sample shows a low conductivity of 0.5 S/cm, similar to that reported in earlier literature.[21] The sample of PPy alone shows conducting behavior with maximum conductivity of 1.18 S/cm. However, the DC electrical conductivity of the PPy/GO composite (41.2 S/cm to 75.8 S/cm) is increased dramatically in comparison with that of PPy and GO alone (Fig. 8). Such enhancement of the conductivity of the composite might be attributed to extended H-bonding between the PPy and GO allowing extended π-conjugation in the PPy chains. The polymerization on the surface and pores of GO sheets restricts the twisting of the polymer backbone away from planarity, which plays a major role in enhancing the conductivity. Also there may have π–π stacking between the GO sheets and polymer backbone. Therefore, GO plays an effective role in enhancement of conductivity.

The electrical conductivity of PPy and PPy/GO composite was also measured in the temperature range of 25°C to 150°C. The electrical conductivity increases with temperature showing semiconducting behavior, and the maximum conductivity was found to be 75.8 S/cm for PPy/GO (5 wt.%) at 150°C. However, a slight increase in temperature results in a decrease of conductivity of the PPy/GO composites, which may be due to removal of solvent bound to the polymer chain and low-molecular-weight oligomers. In addition, the sudden increase in temperature initially up to 70°C may be used up in molecular as well as filler orientation instead of electron hopping from highest occupied molecular orbital (HOMO) to lowest unoccupied molecular orbital (LUMO) and hence the decrease in conductivity observed. On the other hand, the conductivity increased from 70°C to 150°C. At high temperature, the mobility of the charge carrier increases with the increase in interchain and intrachain hopping. An increase in interchain and intrachain hopping results in high charge carrier mobility within the composite, which leads to an increase in conductivity at appropriate high temperatures.

PPy/GO films (5% and 10%) on indium tin oxide (ITO)-coated glass, standard calomel electrode (SCE), and Pt wire were used as working electrodes, reference electrode, and counterelectrode, respectively, with 0.1 M KCl solution as supporting electrolyte prepared in 10 mL acetonitrile. All potentials are reported with respect to the reference electrode. The measurements were calibrated using ferrocene as the standard at a scan rate of 50 mV/s.

Figure 9 illustrates the cyclic voltammograms (CVs) of PPy, GO, and PPy/GO composite electrodes with a potential window from −0.2 V to 1.0 V (versus SCE). All potentials are reported with respect to the reference electrode. The PPy/GO composite electrodes exhibit a nearly rectangular CV (Fig. 9b, c), which indicates good charge propagation within the electrode compared with the pure PPy electrodes (Fig. 9a). GO plays an important role in imparting the better electrochemical performances of the PPy/GO nanocomposites.

The galvanostatic charge–discharge curves of PPy and PPy/GO composites are shown in Fig. 10. The average specific capacitance values, C_g (F/g), of the samples were estimated from the discharge process according to the following equation:

$$C_g = \frac{I\Delta t}{\Delta V \times m}, \tag{5}$$

where I is the current loaded (A), Δt is the discharge time (s), ΔV is the potential change during discharge process, and m is the mass of active material in a single electrode (g).

The galvanostatic charge–discharge curves of PPy and PPy/GO composites are shown in Fig. 10. The mass of active material used for PPy, PPy/GO (5%), and PPy/GO (10%) electrode was 4.3 mg, 10.8 mg, and 11.2 mg, respectively. The discharge curve of the supercapacitor with PPy/GO (5%) composite electrode is similar to that of the supercapacitor with PPy/GO (10%) composite electrode. However,

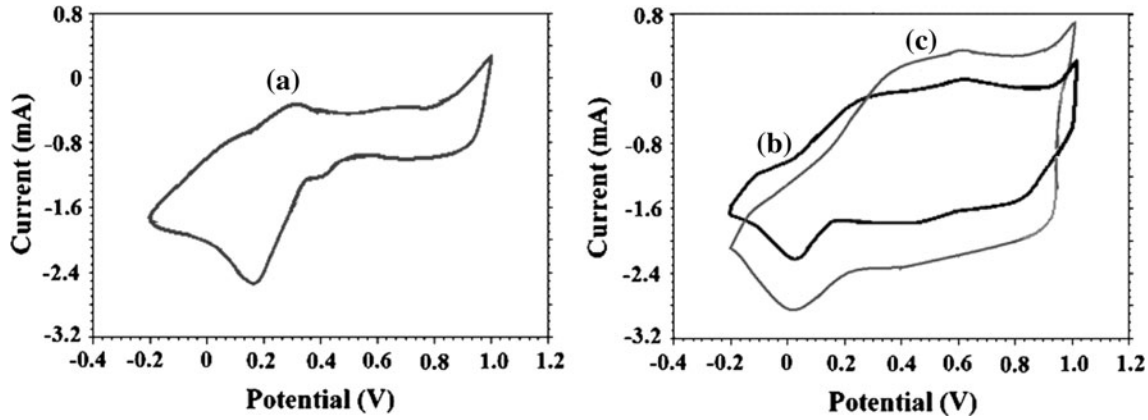

Fig. 9. Cyclic voltammogram of (a) pure PPy, (b) PPy/GO (5%), and (c) PPy/GO (10%) pellet electrode at a scan rate of 50 mV/s.

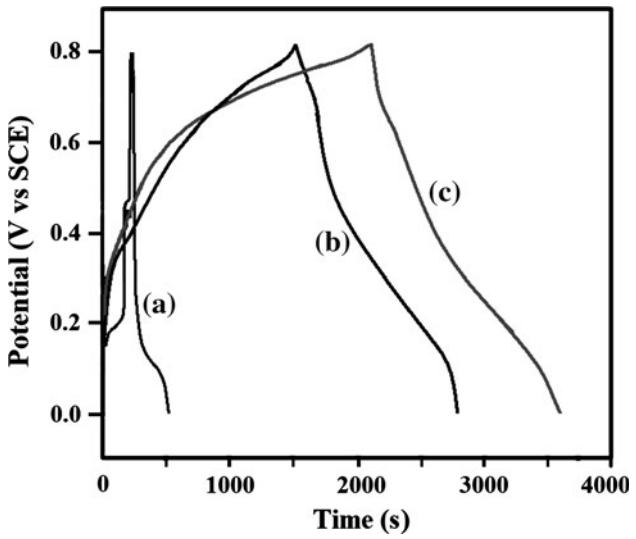

Fig. 10. Galvanostatic discharge curve at 2 mA of (a) pure PPy, (b) PPy/GO (5%), and (c) PPy/GO (10%) pellet electrode.

the "*IR* drop" for the PPy/GO (5%) sample is slightly higher than that of the PPy/GO (10%) supercapacitor. This result reflects that the internal resistance of the PPy/GO (5%) composite (335 Ω) is slightly higher than that of the latter (315 Ω).[22,23] Low internal resistance is of great importance in energy-storage devices, as less energy will be wasted in producing unwanted heat during charging/discharging processes. Thus, incorporating a higher percentage of graphene into the PPy matrix is more suitable for fabricating safe and power-saving supercapacitors compared with PPy alone.

The discharge specific capacitance values of the PPy/GO composite electrodes increased from 370.37 F/g for PPy/GO (5%) to 421.42 F/g for PPy/GO (10%), while the specific capacitance of PPy alone is only 237.20 F/g at 2 mA current in the range from 0 V to 0.80 V. The improved specific capacitance behavior of the PPy/GO composites is due to the presence of GO in the PPy matrix, which allows the counterions to penetrate readily into the polymer matrix and access the internal surface. In addition, the enhanced electrochemical performance of PPy/GO may be due to the synergistic effect between GO and PPy. It is noteworthy that PPy/GO (10%) shows better electrochemical capacitance compared with PPy/GO (5%).

CONCLUSIONS

We successfully prepared a high-performance electrode material based on polypyrrole doped with graphene oxide sheets by *in situ* polymerization. FTIR and XRD revealed the incorporation of GO into the PPy matrix. UV–visible study showed the characteristic redshift of PPy/GO nanocomposites due to the extended conjugation of PPy chains. The electrical conductivity of the composites increased from 41.2 S/cm to 75.8 S/cm with increasing GO and temperature compared with the conductivity of pure PPy (1.18 S/cm). The specific capacitance of the PPy/GO composite electrodes reached 421.4 F/g. With remarkably enhanced specific capacitance compared with polymer alone, the PPy/GO composite electrode can be considered a promising candidate for future development of safe and cost-effective electrochemical supercapacitors.

ACKNOWLEDGEMENTS

The authors would like to thank the Department of Atomic Energy (DAE) and the Board of Research in Nuclear Sciences (BRNS), India, for their financial support of this research under Contract No. 2008/37/37/BRNS/2470.

REFERENCES

1. P. Sen and A. De, *Electrochim. Acta* 55, 4677 (2010).
2. C. Arbizzani, M. Mastragostino, and B. Scosati, *Handbook of Organic Conductive Molecules and Polymers*, ed. H.S. Nalwa (Chichester: Wiley, 1997), Vol. 4, p. 595.
3. W.R. Cieslak (ed.), *Selected Battery Topics, PV 98-15*. The Electrochemical Society (Proceedings Series, Pennington, NJ, 1998).
4. Y.G. Wang, H.Q. Li, and Y.Y. Xia, *Adv. Mater.* 18, 2619 (2006).
5. P. Simon and Y. Gogotsi, *Nat. Mater.* 7, 845 (2008).
6. B.E. Conway, *Electrochemical Supercapacitors: Scientific Fundamentals and Technological Applications* (New York: Kluwer Academic/Plenum, 1999).

7. C. Yang and P. Liu, *Synth. Met.* 160, 768 (2010).
8. J. Wang, Y. Xu, Xi. Chen, and X. Sun, *Compos. Sci. Technol.* 67, 2981 (2007).
9. G. Dione, M.M. Dieng, J.J. Aaron, H. Cachet, and C. Cachet, *J. Power Sources* 170, 441 (2007).
10. L.Z. Fan, Y.S. Hu, J. Maier, P. Adelhelm, B. Smarsly, and M. Antonietti, *Adv. Funct. Mater.* 17, 3083 (2007).
11. L. Li, H. Song, Q. Zhang, J. Yao, and X. Chen, *J. Power Sources* 187, 268 (2009).
12. V. Gupta and N. Miura, *Electrochim. Acta* 52, 1721 (2005).
13. V. Gupta and N. Miura, *J. Power Sources* 157, 616 (2006).
14. J. Jang, J. Bae, M. Choi, and S.H. Yoon, *Carbon* 43, 2730 (2005).
15. A. Rudge, J. Davey, I. Raistrick, S. Gottesfeld, and J.P. Ferraris, *J. Power Sources* 47, 89 (1994).
16. A. Rudge, I. Raistrick, S. Gottesfeld, and J.P. Ferraris, *Electrochim. Acta* 39, 273 (1994).
17. T.M. Wu and S.H. Lin, *J. Polym. Sci. Part A Polym. Chem.* 44, 6449 (2006).
18. M.J. McAllister, J.L. Li, D.H. Adamson, H.C. Schniepp, A.A. Abdala, J. Liu, H.A. Margarita, D.L. Milius, R. Car, R.K. Prud'homme, and I.A. Aksay, *Chem. Mater.* 19, 4396 (2007).
19. C. Gomez-Navarro, R.T. Weitz, A.M. Bittner, M. Scolari, A. Mews, M. Burghard, and K. Kern, *Nano Lett.* 7, 3499 (2007).
20. J. Wu, W. Pisula, and K. Mullen, *Chem. Rev.* 107, 718 (2007).
21. C.M. Yang, Y.J. Kim, M. Endo, H. Kanoh, M. Yudasaka, S. Iijima, and K. Kaneko, *J. Am. Chem. Soc.* 129, 20 (2007).
22. L. Hu, J.W. Choi, Y. Yang, S. Jeong, F. La Mantia, L.-F. Cui, and Y. Cui, *Proc. Natl. Acad. Sci. U.S.A.* 106, 21490 (2009).
23. W. Qiong, X. Yuxi, Y. Zhiyi, L. Anran, and S. Gaoquan, *ACS Nano* 4, 1963 (2010).